Research Article

Rapid enrichment of cesium ions in aqueous solution by copper ferrocyanide powder

Yi Ke[1] · Ye Li[1] · Lijun Zhu[1] · Yuzhi Zhou[1] · Dongbin Liu[1]

Received: 18 December 2019 / Accepted: 25 February 2020 / Published online: 2 March 2020
© Springer Nature Switzerland AG 2020

Abstract
In this study, copper ferrocyanide (CuFC) powder was first prepared by co-precipitation method, and the removal rate, sorption capacity and mechanism of sorption cesium on CuFC was investigated. Before and after sorption, the surface morphology and structure of CuFC were characterized systematically by the Fourier transform infrared spectrometer, the X-ray diffraction (XRD), the scanning electron microscope (SEMEDS), and the thermogravimetric analysis. Batch adsorption experiments were carried out to investigate the effects of adsorbent dose, contact time, solution pH, different initial Cs^+ concentrations, temperature and the effect of competitive ions on Cs^+ adsorption. The FTIR spectrum demonstrated that the product had characteristic absorption peaks such as –C≡N, Fe(II)–C≡N and C≡N–Cu(II), and the XRD spectrum was consistent with the CuFC standard spectrum, indicating that the CuFC was was synthesised successfully. And it can be seen from SEM and EDS that the adsorbent exhibits the same regular cubic crystal structure as the metal ferrocyanide. Kinetic parameters were fitted by the pseudo-second order model ($R^2 = 0.999$), and the adsorption process by the CuFC was chemical adsorption. The adsorption isotherms data of CuFC were well-fitted to the Langmuir ($R^2 = 0.974$). The CuFC effectively captured the Cs^+ ion in the presence of K^+ by the effect of competitive ions. Therefore, the CuFC could be effectively used as a potential adsorbent for Cs^+ adsorption from wastewater.

Keywords Copper ferrocyanide · Cesium · Adsorption · Mechanism

1 Introduction

Due to the extensive usage of global nuclear explosion test [1], nuclear power plant [2], and nuclear waste treatment [3], the release of radioactive wastewater has attracted worldwide attention. The radioactive wastewater does great harm to human health and the whole biosphere. Among them, cesium is a highly poisonous radionuclide that has a tremendous impact on environment for a long time [4–6]. Cs^+ in the wastewater can eventually enter the food chain and be ingested by humans, it has become one of the most urgent issues to develop effective materials for highly efficient enrichment of cesium from radioactive wastewater.

An excellent adsorbent material must have some advantages, such as a large specific surface area, a good pore structure, a certain thermal stability, chemical stability, radiation resistance and so on [7]. Among many adsorbent materials, the ion exchange adsorbent can better meet the enrichment demand of marine radioactive cesium. The inorganic ion exchange sorbent has superiorities of good mechanical properties and radiation resistance, easy operation and more uniform ion exchange position. The adsorption selectivity for Cs^+ is high, and there are many researches on the treatment of high-level liquid waste [8]. The inorganic ion exchange adsorbents used for the adsorption of Cs^+ in seawater mainly include inorganic

✉ Ye Li, whly1218@126.com | [1]School of Resources and Environmental Engineering, Wuhan University of Technology, Wuhan 430070, China.

minerals [9], polyvalent metal phosphates [10], and metal ferrocyanides [11–13].

Although inorganic minerals can be used for the adsorption of radioactive Cs^+ in water, it mostly takes hours or even days to complete the adsorption equilibrium of inorganic mineral adsorbing materials, so it is difficult to meet the timeliness requirements for rapid enrichment detection of marine radionuclides [14]. Multivalent metal phosphates, such as phosphopeptides [15], zirconium phosphates [16], etc., have excellent physicochemical properties and ion exchange capacity, and have good selective adsorption characteristics for alkali metal ions. However, polyvalent metal phosphate ion exchange adsorption materials also have the problem of being susceptible to coexisting ions. Because seawater contains a large amount of cations such as K^+ and Na^+, it directly affects the adsorption efficiency and applicable field of Cs^+ in seawater [17, 18].

Metal ferrocyanide (Prussian blue compound) has a cubic crystal form and the interior is a cavity structure, the different interstitial ions in the crystal lattice are classified into two types, soluble and insoluble [19–23]. The soluble metal ferrocyanide formula can be expressed as $K_nM[Fe(CN)_6]$, and its water dispersibility is superior to the insoluble metal ferrocyanide. Among them, the transition metal ferrocyanide has extremely high chemical stability, its lattice and hydrated Cs^+ size match, and strong adsorption for Cs^+, which is a kind of highly promising radioactive Cs^+ adsorbent. Among the ferrocyanides of different transition metals, zinc, copper and nickel ferrocyanide have better adsorption capacity for Cs^+ [24–28].

Here, copper ferrocyanide powder was synthesized by coprecipitation. The prepared CuFC powder was used as an adsorbent to adsorb Cs^+ ions in radioactive wastewater, by batch sorption technique to assess the adsorbability of CuFC from radioactive wastewater [29–32]. The sorbent was characterized by X-ray diffractometry XRD, infrared spectroscopy FT-IR, scanning electronmicroscope (SEM), energy dispersive spectrometer (EDS) and thermogravimetric analysis (TGA). In addition, batch adsorption experiments were carried out to evaluate the adsorption behavior under different experimental conditions, such as adsorbent dosage, temperature, contact time, solution pH, initial cesium concentration, and the influence of competitive ions(K^+, Na^+, Ca^{2+} and Mg^{2+}). Finally adsorption kinetics and thermodynamic studies were performed to understand the adsorption mechanism.

2 Experimental section

2.1 Preparation of CuFC powder

Synthesis of CuFC: The $Cu(NO_3)_2$ (0.0776 mol/L) solution was slowly added to the $K_4Fe(CN)_6$ (0.1 mol/L) solution under magnetic stirring at 2000 rpm. A dark red precipitate was immediately produced and stirring was continued for 5 min to form a stable suspension. The suspension was placed in a 50 mL sample tube and then centrifuged at 8500 rpm for 10 min. After removing the supernatant, the resulting reddish brown precipitate was washed with deionized water. This process was repeated 2–3 times until the supernatant was clear.

2.2 Characterization of CuFC powder

The surface morphology and structure of CuFC powder were characterized systematically using the scanning electron microscope (SEM–EDS, JSMIT300, Japan Electronics Corporation). Fourier transform infrared spectrometer (FT-IR, Nicolet 6700, America) was used to recorded from 400 to 4000 cm^{-1}. X-ray diffractometry patterns (XRD) of copper ferrocyanide powder before and after adsorption were acquired using a X-ray diffractometer (RU-200B/D/MAX-RB, Japan). Thermogravimetric Analysis (TGA, STA449F3) measurements were conducted by using a TGA thermogravimetric analyzer from 38 to 600 °C at a heating rate of 10 °C.

2.3 Sorption experiments

Cs^+ sorption on CuFC was performed by batch sorption technique at 298 K. The sorbents and adsorbates solution were added in polyethylene tubes to achieve required concentrations of various constituents. The suspension was adjusted to required pH values by adding trace amounts of 0.1 or 0.01 mol/L HCl or NaOH, and then shaken for 3 h to get fully sorption equilibrium. After that, sorbents were separated from liquid phases by a centrifugal separation method. The concentration of Cs^+ was determined by atomic absorption spectrophotometric method. Sorbed amounts of Cs^+ onto CuFC were calculated from the difference between the starting concentration (C_0, mg/L) and the balance concentration (C_e, mg/L) ($q_e = (C_0V_0 - C_eV_e)/m$ and $\eta = (C_0V_0 - C_eV_e) \times 100\%/C_0V_0$, where q_e is the adsorption capacity and η is removal rate, m (g) is the mass of CuFC, V_0 is the initial volume of solution, V_e is the diluted solution volume. All the experimental data were the average of duplicate determinations, and the average uncertainties were < 5%.

3 Results and discussion

3.1 Effect of sorbent content

Cs^+ sorption onto CuFC at various solid contents is shown in Fig. 1. The maximum adsorption amount appeared at 0.4 g/L. At this time, the adsorption rate of CuFC to Cs^+ was 58.12%, and the adsorption amount was 15.2 mg/g, cesium distribution coefficient was lgKd = 3.5 ± 1.0 ml/g. Compared with other types of ferrocyanide in Table 1, copper ferrocyanide can effectively enrich cesium ions from low concentration wastewater (the initial concentration 10 mg/L) especially when the dosage is 2.0 g/L, the adsorption rate reaches 96.74%。 The reason for the above phenomenon may be that as the CuFC powder in the system increases, the active adsorption sites increase, and more Cs^+ is adsorbed on the surface of the adsorbent, so the adsorption rate increases. However, since the total amount of Cs^+ is constant and the adsorbents collide and aggregate after increasing, the active site of the unit mass adsorbent decreases, so the unit adsorption amount also decreases [36]. For practical application in radioactive wastewater treatment, the optimal dosage for CuFC under similar condition is 2.0 g/L.

3.2 Effect of initial pH on Cs^+ sorption

The sorption of Cs^+ on CuFC was greatly influenced by the solution pH (Fig. 2). The sorption increased from about 76 to 99.3% when the pH value increased from 1.0 to 7.0, and maintained the high level at pH 7.0–9.0, then decreased steeply from 99.3 to 84.5% in the pH range of 9.0–13.0. The reason for the low adsorption performance under acidic conditions(pH = 1–5) was mainly due to the competitive adsorption between H^+ and Cs^+ in the solution, occupying the adsorption site, which greatly affected the adsorption process. Under weak alkaline or neutral conditions (pH = 7–9), the H^+ competitive adsorption was weakened, and the adsorption capacity of CuFC to Cs^+ was higher. With the increase of alkalinity(pH > 9), the OH^- in the solution increases continuously, and there was a strong force between Fe^{3+} and OH^-, which caused the Fe–CN–Cu bond in the CuFC to break and the material structure was destroyed, so the adsorption effect was lowered.

3.3 Effect of sorbent contact time

Figure 3 showed the effect of contact time on Cs^+ adsorption. During the whole adsorption process, the adsorption rate was the fastest in the first 50 min, and the adsorption

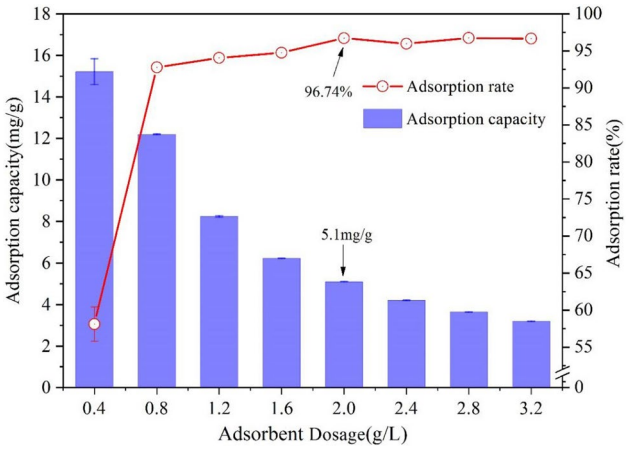

Fig. 1 Effect of CuFC dosage on Cs^+ adsorption (v = 25 mL, T = 298 K, pH = 7)

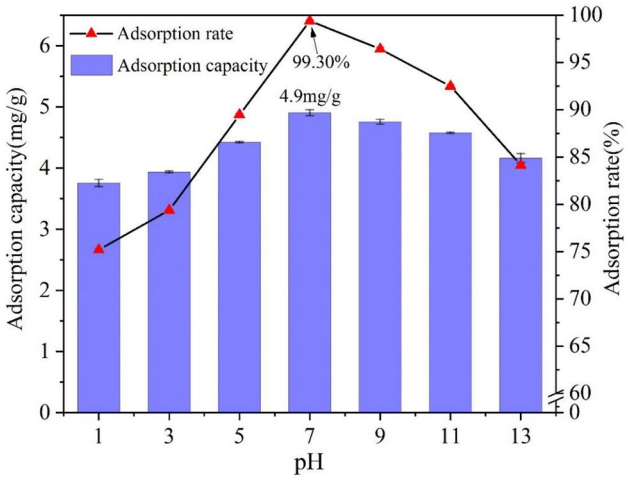

Fig. 2 Effect of pH of reaction system on adsorption of Cs^+ (v = 25 mL, m = 0.05 g, T = 298 K)

Table 1 Comparison of different types of ferrocyanide

Materia	Kd (ml/g)	q (mg/g)	References
Copper ferrocyanide	3.5 ± 1.0	15.2	–
Tripolite and nickel(II) ferrocyanide	4.2	–	[33]
Nickel potassium-clinoptilolite of the Shivertui	7.0 ± 1.0	500 ± 60	[34]
Nickel potassium-glauconite	5.0 ± 0.3	220 ± 23	[34]
Nickel-potassium ferrocyanide-clinoptilolite	4.5 ± 0.4	–	[35]

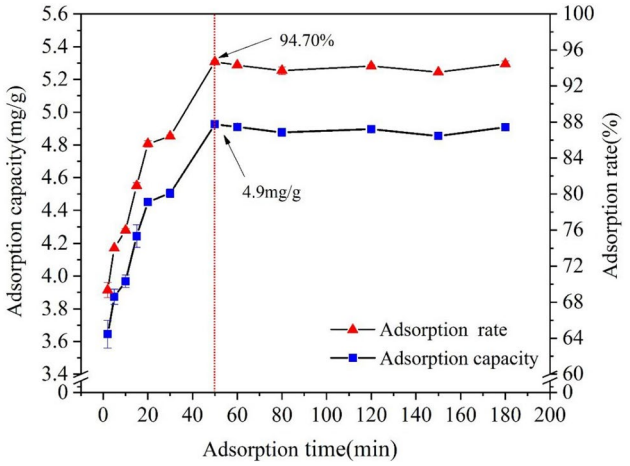

Fig. 3 Effect of contact time on adsorption of Cs+ (v = 25 mL, m = 0.05 g, T = 298 K, pH = 7)

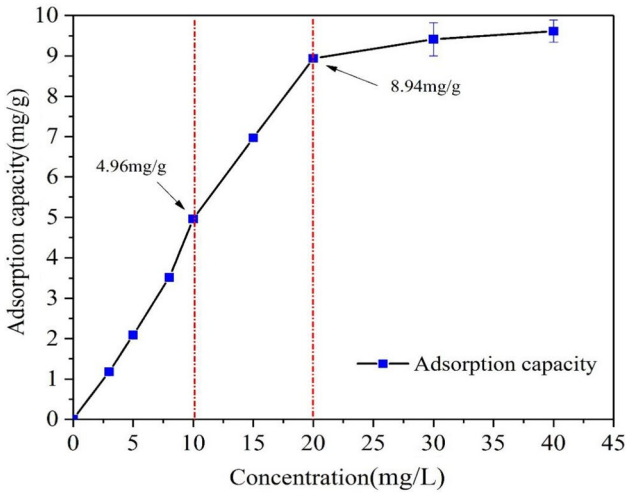

Fig. 4 Effect of initial concentration on adsorption of Cs^+ (v = 25 mL, m = 0.05 g, T = 298 K, pH = 7)

capacity increased significantly. After 50 min, the adsorption gradually became equilibrium. At this time, the adsorption amount and adsorption rate of Cs^+ were about 4.9 mg/g and 94.70%, respectively.

This was because in the initial stage of adsorption, since the adsorbent material had more active sites, Cs^+ was rapidly adsorbed to the active site. In the middle of adsorption, as the active site was continuously occupied, the Cs^+ adsorbed on the material had a resistance to the diffusion of Cs^+ in the solution, which make it difficult for Cs^+ to diffuse into the interior of the particle, so the adsorption process was slow. In the late stage of adsorption, when the active sites were all occupied by Cs^+, the adsorption reached equilibrium.

3.4 Effect of initial concentration of Cs^+

It can be seen apparently from Fig. 4 that the adsorption rate of CuFC to Cs^+ was increased with the Cs^+ initial concentration and then reached equilibrium. This was because the adsorption of Cs^+ by CuFC was not saturated at low concentration, the contact probability of adsorbent with Cs^+ was small, and under the effect of increasing concentration driving force, when the concentration increased, the contact between adsorbent and Cs^+ were increased. The amount of adsorption of Cs^+ on the material was increasing. Thereafter, the initial concentration of the solution was further increased, and since the adsorbent material contained a certain number of active sites, the adsorption capacity for Cs^+ was also limited. At this time, the initial concentration of the solution was increased, and the active sites of the adsorbent material were all occupied, so the adsorption amount hardly changed, and the adsorption tended to be saturated.

3.5 Effect of coexisting ions

Interfering ions can affect the presence and activity of metal ions. The effect of common cations K^+, Na^+, Ca^{2+} and Mg^{2+} on the adsorption of Cs^+ by CuFC was shown in Fig. 5. Among them, K^+ and Na^+ showed a slight inhibitory effect on Cs^+ adsorption. With the increased of K^+ and Na^+ ionic strength, the adsorption capacity and adsorption rate of Cs^+ were decreased slightly, and the inhibitory effect of K^+ was slightly stronger than Na^+. When the concentration was increased from 0 to 400 mg/L, the adsorption amount of Cs^+ decreased by 0.16 mg/g, and the adsorption rate decreased by 4.6%. Under the same conditions of Na^+, the adsorption amount of Cs^+ decreased by only 0.11 mg/g, and the adsorption rate decreased by 3.5%. The presence of Ca^{2+} and Mg^{2+} hardly inhibited the adsorption of Cs^+. This may be caused by the difference in the hydration radius of the ions. closer to the Cs^+ hydration radius, the stronger the competitive adsorption capacity. (Cs^+ hydration radius is 3.25 Å, K^+ and Na^+ are close to 3.3 Å, 3.6 Å, Ca^{2+} is 4.1 Å, and Mg^{2+} is 4.25 Å [37]). K^+ and Cs^+ had similar ionic radii and hydration energy. During the adsorption process, K^+ will compete with Cs^+ for a limited adsorption site, resulting in a decrease of adsorption capacity, but this inhibition was very limited. CuFC had good anti-interference in salty solutions.

3.6 Adsorption kinetics

In order to clarify the sorption process of cesium in CuFC, the pseudo-first-order kinetic model and the pseudo-second-order kinetic model were applied to analysis the

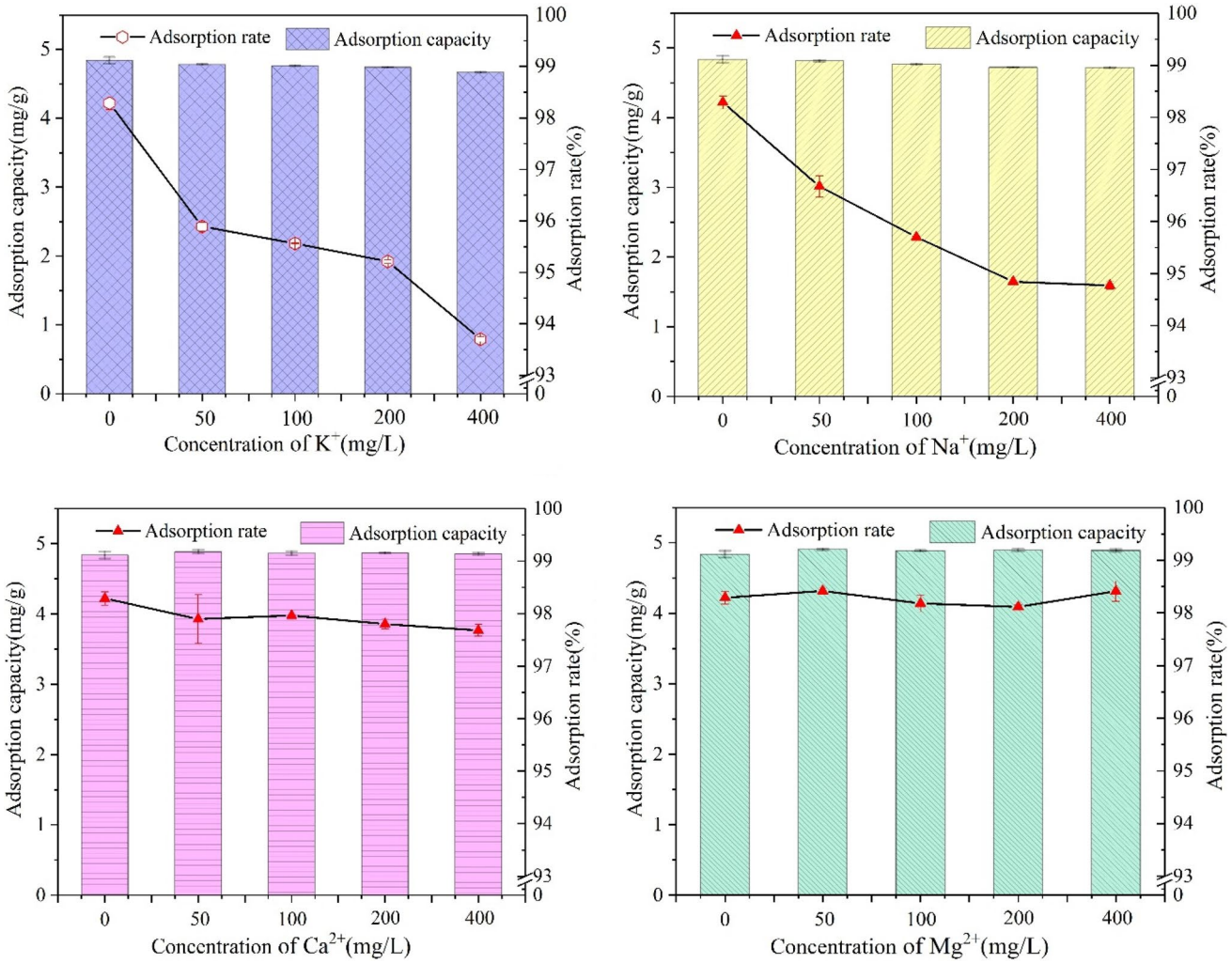

Fig. 5 Effect of common cations on adsorption of Cs^+ (v = 25 mL, m = 0.05 g)

experimentally observed kinetic data, their linear form can be expressed as:

First order kinetic model:

$$ln(q_e - q_t) = lnq_e - k_1 t \quad (1)$$

Second order kinetic model:

$$\frac{t}{q_t} = \frac{t}{q_e} + \frac{1}{k_2 q_e^2} \quad (2)$$

where q_e is the sorption amount at equilibrium (mg/g), q_t is the sorption amount at t (mim), k_1 is the rate constant (min^{-1}), and k_2 is the rate constant of second-order Kinetic model (g mg^{-1} min^{-1}).

Figure 6 showed that the first-order kinetic model ($R^2 = 0.54$) and the pseudo-secondary kinetic model ($R^2 = 0.999$) were used to research the reaction kinetics of cesium on CuFC. In the adsorption process, the fitting effect of the first-order kinetic model was not good, and the linear fitting correlation coefficient R^2 was not high; However, the pseudo-secondary kinetic model has a good fitting effect ($R^2 = 0.999$), and the relative error between the theoretical adsorption value and the experimental value of Cs^+ was small. It showed that the adsorption of Cs^+ by CuFC was a heterogeneous diffusion process, and there were many reaction mechanisms, not a simple first-order reaction.

3.7 Adsorption isotherm

Adsorption isotherm are mathematical models that describe how adsorbates interact with adsorbents. In this study, all the experimental date were analyzed according to the two common nonlinear: Freundlich and Langmuir. The Langmuir model in Fig. 7a shown that the maximum adsorption capacity of CuFC for cesium was 11.12 mg/g,

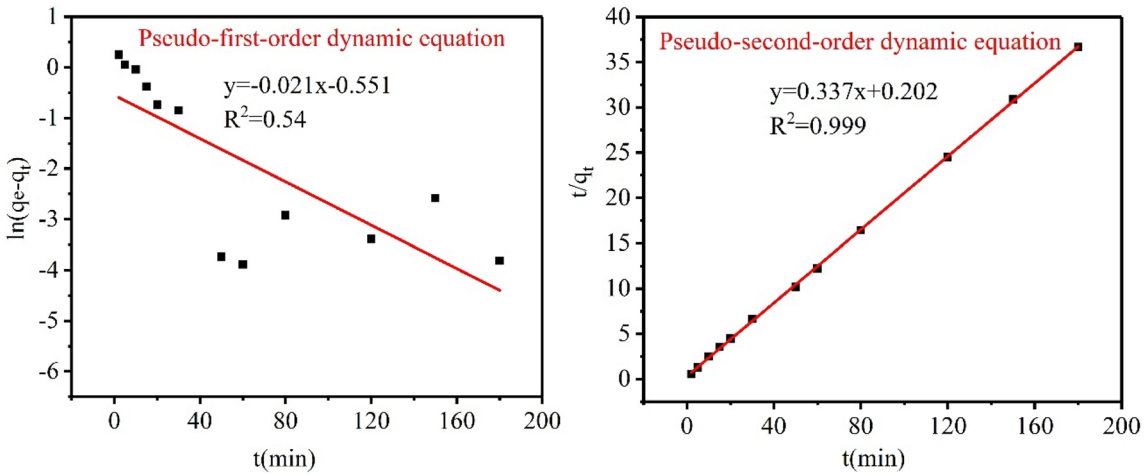

Fig. 6 Adsorption kinetic model fitting for adsorption of Cs^+ on CuFC (v = 25 mL, m = 0.05 g)

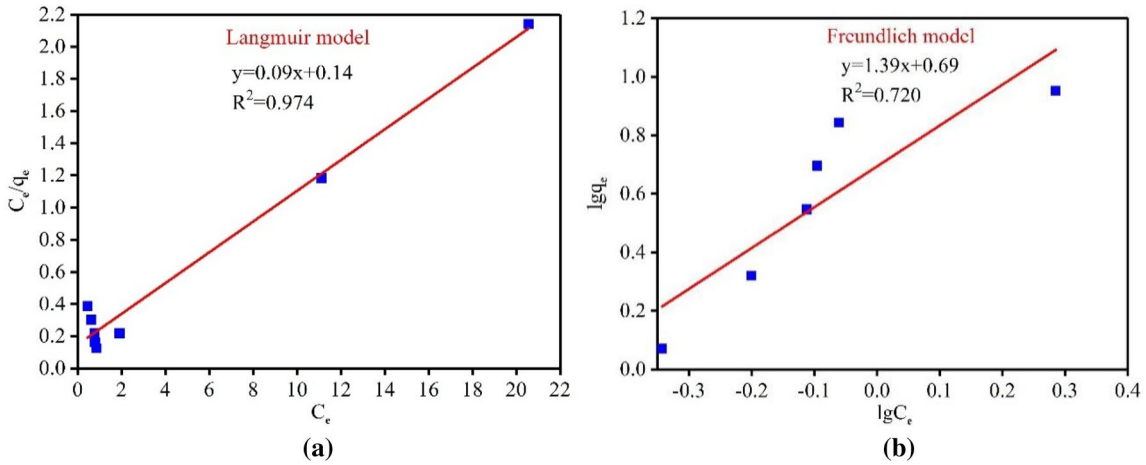

Fig. 7 Adsorption isotherm model of CuFC for Cs^+ at 25 °C (v = 25 mL, m = 0.05 g)

and the R_L was 0.610 ($0 < R_L < 1$) when the initial concentration was 10 mg/L, suggesting that CuFC had higher affinity for cesium and also it was beneficial to promote the reaction. The Freundlich model in Fig. 7b shown that the characteristic constant n was 0.72 ($1 < n < 10$), indicating that the adsorption of Cs^+ by CuFC does not conform to the Freundlich model.

Table 2 listed the separation factor R_L of Cs^+ adsorbed by CuFC at different concentrations at 298 K, and the values were all between 0 and 1, indicating that the adsorption of Cs^+ by CuFC belonged to preferential adsorption (favorable adsorption).

3.8 Characterization of CuFC powder

3.8.1 FTIR spectra of CuFC

Figure 8 showed the FTIR spectrum of EPS before and after adsorption. At 2090 cm^{-1}, there was a sharp peak of –C≡N, which showed a blue shift compared to the characteristic peak of free cyano (The free cyano characteristic peak usually appears at 2600 cm^{-1}), This was because the cyano group was combined with metal ions, which provide electrons to the metal ions [38]. The sharp characteristic peak appearing at around 592 cm^{-1} was the deformation

Table 2 Separation factor of Cs^+ (R_L)

C_0	3	5	8	10	15	20	30	40
R_L	0.25	0.17	0.11	0.09	0.06	0.05	0.03	0.02

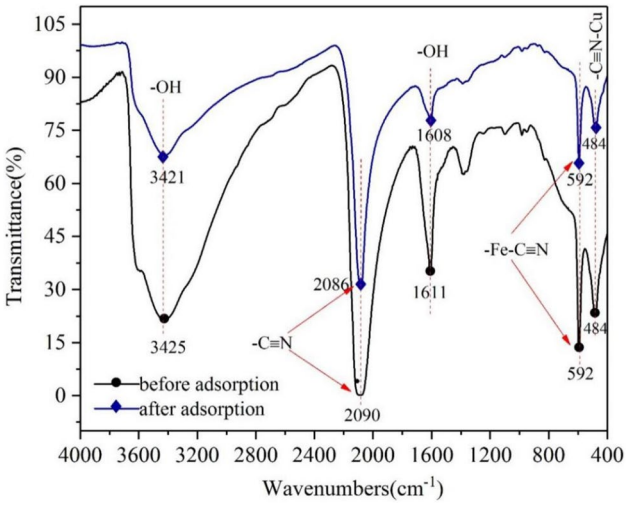

Fig. 8 FT-IR spectras of CuFC before and after adsorption of Cs^+

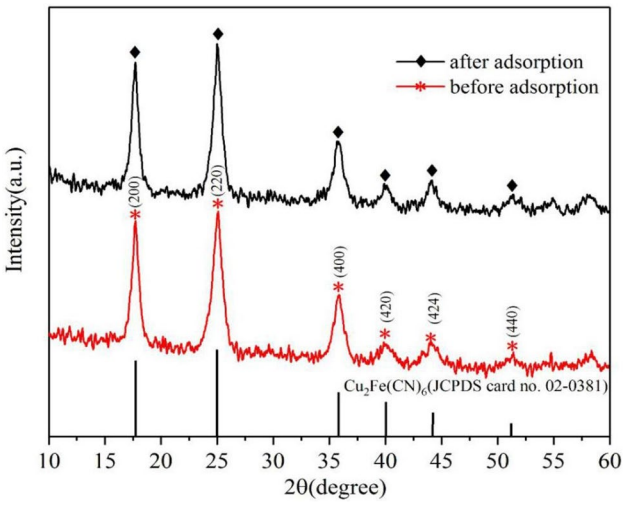

Fig. 9 XRD spectras of CuFC before and after adsorption of Cs^+

vibration absorption peak of –Fe(II)–C≡N, and the characteristic peak appearing at around 484 cm^{-1} was the deformation vibration absorption peak of –C≡N–Cu(II). The characteristic peaks appearing in the above three points showed that the synthesized powder had obvious characteristic peaks of CuCF, and the deformation vibration in the plane of Fe(II)–C≡N–Cu(II) was formed, and the CuCF powder was successfully synthesized. In addition, at 3425 cm^{-1}, a broad and strong peak was the stretching vibration peak of O–H, and the absorption peak at 1611 cm^{-1} was the stretching vibration peak of O–H. These two characteristic peaks may be attributed to the presence of water molecules in the material gap.

3.8.2 XRD spectra of CuFC

Figure 9 showed the XRD spectrum of CuFC before and after adsorption. The synthesized CuFC powder had a sharp diffraction peak at 2θ of 10°–60°, indicating that the compound had good crystallinity. Both the two samples displayed six characteristic peaks at 2θ = 17.7°, 25.2°, 35.7°, 40.4°, 44.3°, 51.9°, corresponding to 200, 220, 400, 420, 424, 440 diffractive surfaces. The pattern was consistent with the standard pattern of copper ferrocyanide (JCPDS card no. 02–0381), and it can be determined that the synthesized powder was CuFC. In addition, the diffraction peak appeared at 55.7° of the XRD pattern may be an impurity peak remaining during the synthesis of copper ferrocyanide.

3.8.3 FE-SEM and EDS image of CuFC

Figure 10 showed the SEM spectra of CuFC before and after adsorption. The shape of CuFC before and after adsorption was irregular, the size was about 50–200 nm and there was serious agglomeration. The surface of the CuFC before adsorption was rough, which was favorable for the adsorption point exposure to promote adsorption. After adsorption of Cs^+, the surface porosity of the material decreased, and the overall tended to be regular. In the scanning electron micrographs before and after adsorption, cubic CuFC with sharp edges and corners can be distinguished, and the particle size was about several tens of nanometers.

As shown in Fig. 11a that the surface of CuFC was detected to contain elements such as N, K, Fe, and Cu and so on before adsorption, but Cs was not detected. C was not detected because the conductive paste used contains C element, and the scanning signal of C in CuFC coincided with the signal of C in the conductive paste. After adsorption, it can be clearly seen from Fig. 11b that the orange-red Cs signal appeared on the surface of CuFC. In Fig. 12 showed that the content of the K decreased as 2.75%, and the content of Cs was increased by 2.61%. The content of other elements before and after adsorption had not changed significantly. The results were consistent with previous studies [39]. It can be speculated that the adsorption of Cs^+ by CuFC may be mainly caused by ion exchange between K^+ and Cs^+ inside the structure. The main adsorption mechanism is shown in Fig. 13.

3.8.4 TGA-DTG curvers of CuFC

The TG curve of copper ferrocyanide showed a gradient change (Fig. 14), which can be roughly divided into four stages: I (38–155 °C), II (155–220 °C), III (220–320 °C), IV (320–600 °C). The copper ferrocyanide structure containe

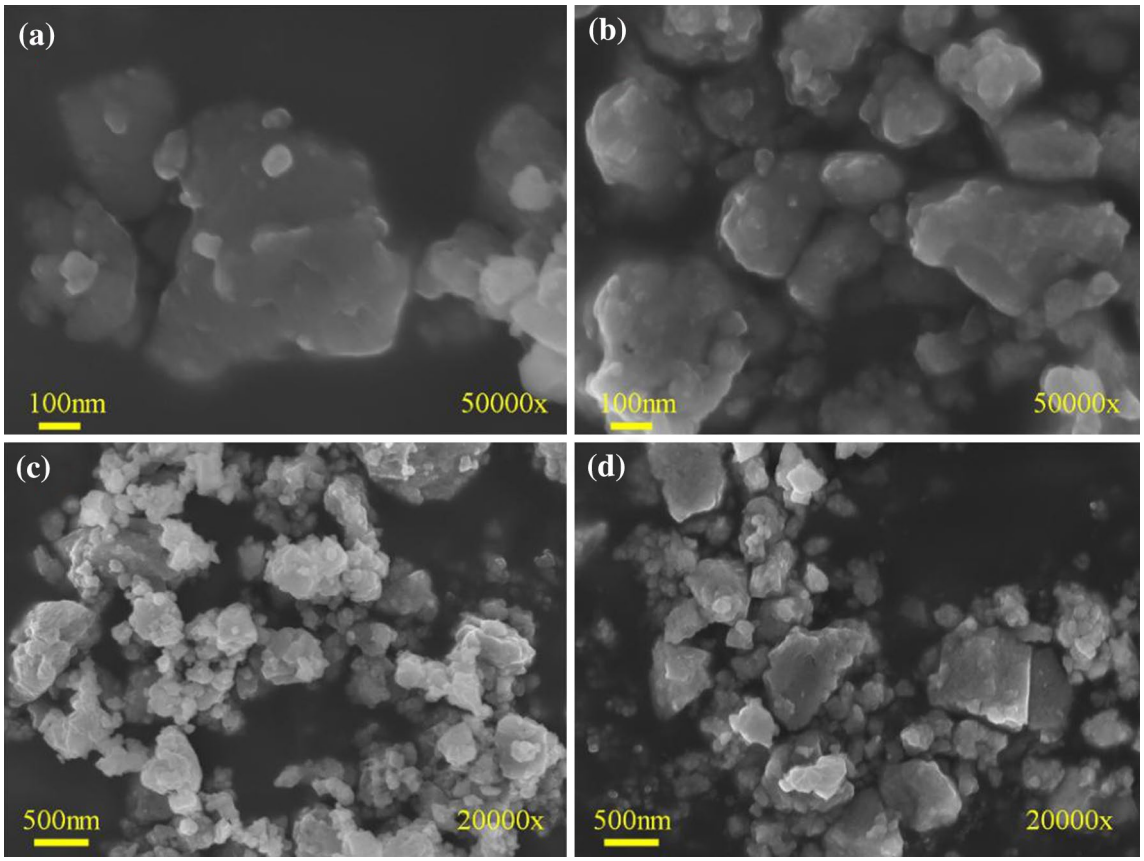

Fig. 10 CuFC powders with different magnification before and after adsorption (**a**, **c** before adsorption; **b**, **d** after adsorption)

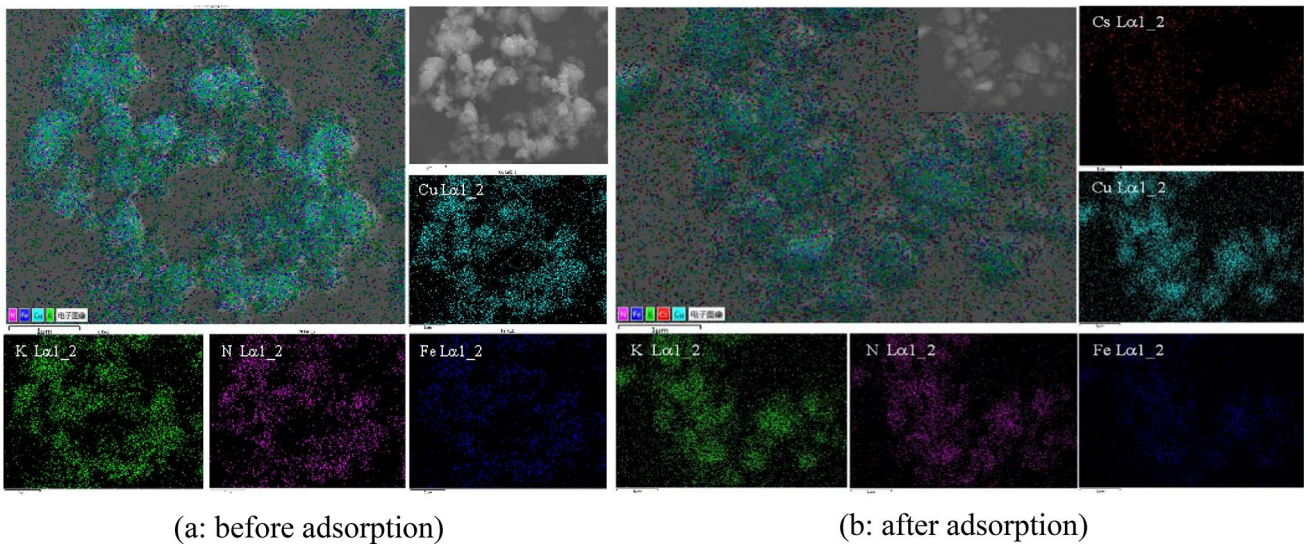

Fig. 11 EDS layer diagram of CuFC before and after Cs^+ adsorption

two kinds of water: one is the structurally adsorbed zeolite water, and the other is the coordination water in the structure [40]. In stage I, the adsorbed water, zeolite water, etc. on the surface of the material were evaporated and the mass loss was about 20%; the mass loss in stage II was 11%, which may be attributed to the release of the

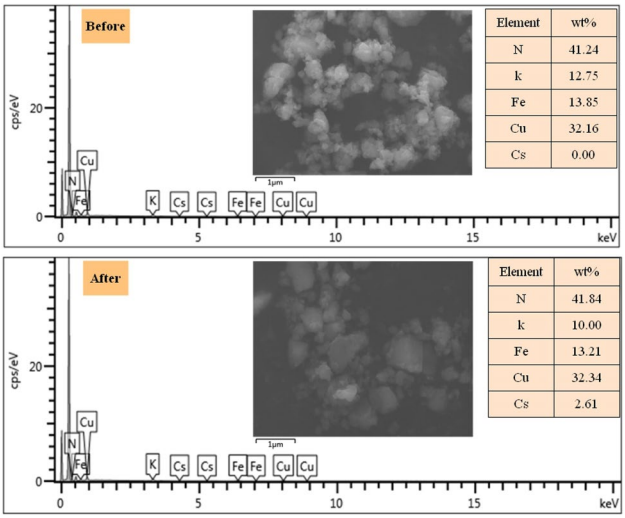

Fig. 12 EDS total spectrum of CuFC before and after Cs^+ adsorption

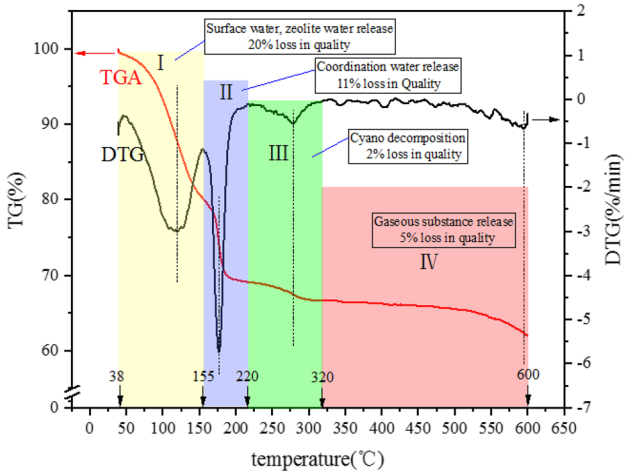

Fig. 14 TGA-DTG curves of CuFC

coordination water in the material structure. The above two-stage temperature rise did not cause a change in the crystal structure of the material, and the mass loss was actually a water loss process of the material. The temperature in stage III, the crystal structure of copper ferrocyanide was broken, and C≡N was broken and decomposed [41], causing about 2% mass loss. The temperature in the IV stage continued to rise, and intermediate products due to structural damage of the material are produced. About 5% of the mass loss may be caused by the escape of gases such as CO_2 and NO_2 [42].

4 Conclusions

CuFC was prepared by co-precipitation method. The result of FTIR of the obtained product showed obvious absorption peak of CuFC. The XRD pattern was consistent with the standard spectrum, indicating that CuFC was successfully synthesized. The results obtained from XRD, FTIR, SEM and EDS showed that the appearance, chemical composition and atomic bonding mode of CuFC before and after adsorption did not change significantly. The mass loss of K element was basically consistent with the increase of mass of Cs element, while the mass fraction of other elements

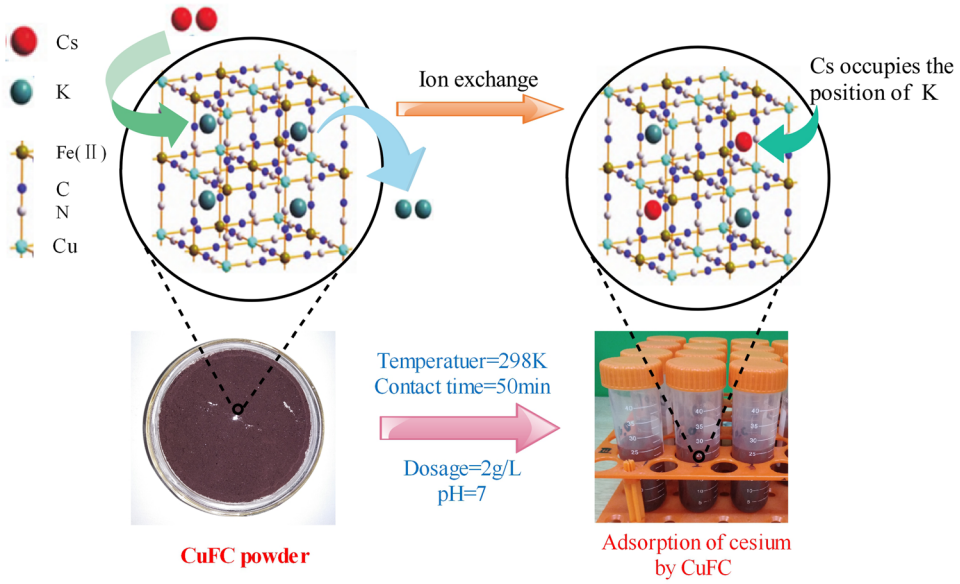

Fig. 13 Main adsorption mechanism of Cs^+ by CuFC

$$K_2\text{-}CuFe(CN)_6 + Cs^+ \rightarrow Cs_2\text{-}CuFe(CN)_6 + K^+$$

such as N, Fe and Cu did not change significantly. CuFC adsorption on Cs^+ was caused by ion exchange between K^+ and Cs^+ in its structure. TGA analysis showed that CuFC had good thermal stability.

Acknowledgements This work was supported in part of the project titled "The National Key roject of Research and Development Plan" (Grant No. 2016YFC1402504). The all authors are grateful to financial support for this study.

Compliance with ethical standards

Conflict of interest The authors declare that there is no any conflict of interest regarding the publication of this article.

References

1. Aarkrog A (2003) Input of anthropogenic radionuclides into the World Ocean. Deep Sea Res II 50:2597–2606
2. Buesseler K, Dai M, Aoyama M, Benitez-Nelson C, Charmasson S, Higley K, Maderich V, Masque P, Oughton D, Smith JN (2017) Fukushima Daiichi-derived radionuclides in the ocean: transport fate, and impacts. Ann Rev Mar Sci 9:173–203
3. Jones SR, Lambers B, Stevens A (2004) Disaggregation of collective dose—a worked example based on future discharges from the Sellafield nuclear fuel reprocessing site UK. J Radiol Prot 24:13
4. Fesenko SV, Alexakhin RM, Balonov MI, Bogdevitch IM, Howard BJ, Kashparov VA, Sanzharova NI, Panov AV, Voigt G, Zhuchenka YM (2007) An extended critical review of twenty years of countermeasures used in agriculture after the Chernobyl accident. Sci Total Environ 383:1–24
5. Joel ES, Maxwell O, Adewoyin OO, Ehi-Eromosele CO, Embong Z, Saeed MA (2018) Assessment of natural radionuclides and its radiological hazards from tiles made in Nigeria. Sci Total Environ 144:43–47
6. Harikrishnan N, Ravisankar R, Chandrasekaran A, Gandhi MS, Vijayagopal P, Mehra R (2018) Assessment of gamma radiation and associated radiation hazards in coastal sediments of south east coast of Tamilnadu, India with statistical approach. Ecotoxicol Environ Saf 162:521–528
7. Olatunji MA, Khandaker MU, Mahmud HNME, Amin YM (2015) Influence of adsorption parameters on cesium uptake from aqueous solutions—a brief review. RSC Adv 5:71658–71683
8. Li MC, Zhao JY, Li Y, Li MC, Wu YC, Wang C, Jiao H, Na P (2019) Enhanced adsorption of cesium ions by electrochemically switched ion exchange method: based on surface-synthetic $Na_2Ti_3O_7$ nanotubes. Colloids Surf A 579:123712
9. Yan JS, Li Y, Li HR, Zhou YZ, Xiao HF, Li BL, Ma X (2019) Effective removal of ruthenium(III) ions from wastewater by amidoxime modified zeolite X. Microchem J 145:287–294
10. Shady SA (2009) Selectivity of cesium from fission radionuclides using resorcinol-formaldehyde and zirconyl-molybdopyrophosphate as ion-exchangers. J Hazard Mater 167:947–952
11. Awual MR, Miyazaki Y, Taguchi T, Shiwaku H, Yaita T (2016) Encapsulation of cesium from contaminated water with highly selective facial organic–inorganic mesoporous hybrid adsorbent. Chem Eng J 291:128–137
12. Ojwang DO, Grins J, Wardecki D, Valvo M, Renman V, Haggstrom L, Ericsson T, Gustafsson T, Mahmoud A, Hermann RP, Svensson G (2016) Structure characterization and properties of K-containing copper hexacyanoferrate. Inorg Chem 55:5924–5934
13. Soek RN, Schmidt A, Winnischofer H, Vidotti M (2016) Anisotropic behavior of layer-by-layer films using highly disordered copper hexacyanoferrate(II) nanoparticles. Appl Surf Sci 378:253–258
14. El-Kamash AM (2008) Evaluation of zeolite A for the sorptive removal of Cs^+ and Sr^{2+} ions from aqueous solutions using batch and fixed bed column operations. J Hazard Mater 151:432–445
15. Mack S, Scott AM (2019) Ion/ion charge inversion/attachment in conjunction with dipolar DC collisional activation as a selective screen for sulfo- and phosphopeptides. Int J Mass Spectrom 444:116181
16. Ibrahim Y, Abdulkarem E, Naddeo V, Banat F, Hasan SW (2019) Synthesis of super hydrophilic cellulose-alpha zirconium phosphate ion exchange membrane via surface coating for the removal of heavy metals from wastewater. Sci Total Environ 690:167–180
17. Wang D, Xu YB, Xiao DF, Qiao QG, Yin P, Yang ZL, Li JX, Winchester W, Wang Z, Hayatd T (2019) Ultra-thin iron phosphate nanosheets for high efficient U(VI) adsorption. J Hazard Mater 371:83–93
18. Akkaya R (2012) Removal of radio nuclides of the U- and Th-series from aqueous solutions by adsorption onto polyacryamide-expanded perlite: effects of pH, concentration and temperature. Nucl Instrum Methods Phys Res A 688:80–83
19. Alamudy HA, Cho K (2018) Selective adsorption of cesium from an aqueous solution by a montmorillonite-prussian blue hybrid. Chem Eng J 349:595–602
20. Loos-Neskovic C, Ayrault S, Badillo V, Jimenez B, Garnier E, Fedoroff M, Jones DJ, Merinov B (2004) Structure of copper-potassium hexacyanoferrate(II) and sorption mechanisms of cesium. J Solid State Chem 177:1817–1828
21. Grandjean A, Delchet C, Causse J, Barre Y, Guari Y, Larionova J (2015) Effect of the chemical nature of different transition metal ferrocyanides to entrap Cs. J Radioanal Nucl Chem 307:427–436
22. Nilchi A, Saberi R, Moradi M, Azizpourb H, Zarghami R (2011) Adsorption of cesium on copper hexacyanoferrate–PAN composite ion exchanger from aqueous solution. Chem Eng J 186:572–580
23. Kamenık J, Dulaiova H, Sebesta F, Stastna K (2013) Fast concentration of dissolved forms of cesium radioisotopes from large seawater samples. J Radioanal Nucl Chem 296:841–846
24. Avramenko V, Bratskaya S, Zheleznov V, Sheveleva I, Voitenko O, Sergienko V (2011) Colloid stable sorbents for cesium removal: preparation and application of latex particles functionalized with transition metals ferrocyanides. J Hazard Mater 186:1343–1350
25. Dedovets D, Bauduin P, Causse J, Girard L, Diat O (2016) Switchable self-assembly of prussian blue analogs nano-tiles triggered by salt stimulus. Phys Chem Chem Phys 18:3188–3196
26. Hu M, Furukawa S, Ohtani R, Sukegawa H, Nemoto Y, Reboul J, Kitagawa S, Yamauchi Y (2012) Synthesis of prussian blue nanoparticles with a hollow interior by controlled chemical etching. Angew Chem Int Ed Engl 51:984–988
27. Jang J, Lee DS (2016) Magnetic prussian blue nanocomposites for effective cesium removal from aqueous solution. Ind Eng Chem Res 55:3852–3860
28. Yang HJ, Sun L, Zhai J, Li HY, Zhao Y, Yu HW (2014) In situ controllable synthesis of magnetic prussian blue/graphene oxide nanocomposites for removal of radioactive cesium in water. J Mater Chem A 2:326–332
29. Jang SC, Haldorai Y, Lee GW, Kyu HS, Han YK, Roh C, Huh YS (2015) Porous three-dimensional graphene foam/prussian blue composite for efficient removal of radioactive (137)Cs. Sci Rep 5:17510
30. Lee HK, Choi JW, Oh W, Choi SJ (2016) Sorption of cesium ions from aqueous solutions by multi-walled carbon nanotubes

functionalized with copper ferrocyanide. J Radioanal Nucl Chem 309:477–484
31. Vincent T, Vincent C, Barre Y, Guari Y, Saout GL, Guibal E (2014) Immobilization of metal hexacyanoferrates in chitin beads for cesium sorption: synthesis and characterization. J Mater Chem A 2:10007–10021
32. Egorin A, Tokar E, Zemskova L (2016) Chitosan-ferrocyanide sorbent for Cs-137 removal from mineralized alkaline media. Radiochim Acta 104:657–661
33. Ivanets AI, Shashkova IL, Drozdova NV, Davydov DYu, Radkevich AV (2014) Recovery of cesium ions from aqueous solutions with composite sorbents based on tripolite and copper(II) and nickel(II) ferrocyanides. Radiochemistry 56:524–528
34. Voronina AV, Blinova MO, Kulyaeva IO, Sanin PY, Semenishchev VS, Afonin YD (2015) Sorption of cesium radionuclides from aqueous solutions onto natural and modified aluminosilicates. Radiochemistry 57:522–529
35. Voronina AV, Gorbunova TV, Semenishchev VS (2017) The effect of the synthesis method on the parameters of pore structure and selectivity of ferrocyanide sorbents based on natural minerals. J Radioanal Nucl Chem 312:241–254
36. Sangvanich T, Sukwarotwat V, Wiacek RJ, Grudzien RM, Fryxell GE, Addleman RS, Timchalk C, Yantasee W (2010) Selective capture of cesium and thallium from natural waters and simulated wastes with copper ferrocyanide functionalized mesoporous silica. J Hazard Mater 182:225–231
37. Thammawong C, Opaprakasit P, Tangboriboonrat P, Sreearunothai P (2013) Prussian blue-coated magnetic nanoparticles for removal of cesium from contaminated environment. J Nanopart Res 15:1689
38. Brisdon A (2010) Kazuo Nakamoto infrared and Raman spectra of inorganic and coordination compounds, part B, applications in coordination, organometallic, and bioinorganic chemistry, 6th edn Wiley, 2009, 424 pp. (hardback) ISBN 978-0-471-74493-1. Appl Organomet Chem 24:489
39. Qin YH, Kang B, Dai YD, Li J, Shen WT (2014) Adsorption mechanism analysis of cesium ions nickel hexacyanoferrate. At Energy Sci Technol 48:1751–1756
40. Kiliyankil VA, Yang HB, Bunshi F (2013) Prussian blue caged in alginate/calcium beads as adsorbents for removal of cesium ions from contaminated water. J Hazard Mater 258:93–101
41. Hitoshi M, Jukka L, Risto H (1997) Chemical and thermal stablility of potassium nickel hexacyanoferrate(II). J Nucl Sci Technol 34:582–587
42. Lehto J, Pettersson M, Hinkula J, Rasanen M, Elomaa M (1995) Gases evolved in the thermal decomposition of potassium cobalt hexacyanoferrate(II). Thermochim Acta 265:25–30

Publisher's Note Springer Nature remains neutral with regard to jurisdictional claims in published maps and institutional affiliations.